Electronic Supplementary Material (ESI) for Green Chemistry.

Enzymatic hydrolysis lignin derived hierarchical porous carbon for supercapacitor in ionic liquid with high power and energy density

Nannan Guo, Min Li, Xingkai Sun, Feng Wang*, Ru Yang**

State Key Laboratory of Chemical Resource Engineering, Beijing Key Laboratory of Electrochemical Process and Technology for Materials, Beijing University of Chemical Technology, Beijing 100029, P. R. China

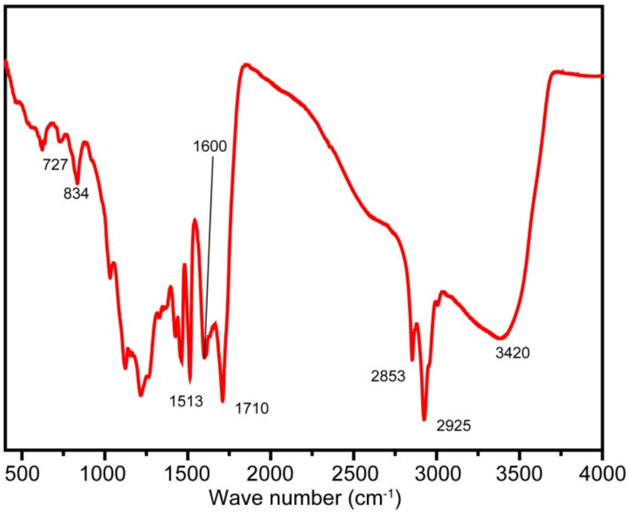

Fig. S1 FTIR spectrum of the enzymatic hydrolysis lignin derived from biobutanol production.

The FTIR spectrum of enzymatic hydrolysis lignin derived from biobutanol production shows a broad band around 3420 cm^{-1}, which can be assigned to the O-H stretching mode of hydroxyl groups. The bands at 2925 and 2853 cm^{-1} belong to -CH$_2$- asymmetric vibration, and the band at 1710 cm^{-1} is due to the stretching vibrations of C=O.[1] The band at 1600 cm^{-1} may be ascribed to the aromatic ring

---

* **Corresponding author**: **E-mail: wangf@mail.buct.edu.cn (F. Wang) Fax: +86 10 64451996;**

** **Corresponding author: E-mail address: ruyang@mail.buct.edu.cn (R. Yang). Fax: +86 10 64436736.**

stretching vibrations (C=C) enhanced by polar functional groups and the band in the 1513 cm^{-1} suggests that aromatic ring bands and double bond (C=C) vibrations overlap the mentioned C=O stretching vibration bands and OH binding vibration bands.[2, 3] Another broad band in the 1470-1330 cm^{-1} region consists of a series of overlapping absorption bands which are ascribable to the deformation vibration of surface hydroxyl groups and in-plane vibrations of CH in various C=CH structures.[4] The band at 1217 cm^{-1} corresponds to the asymmetric stretching of =C-O-C connected with aryl groups in lignin.[5] Two quite weak shoulder peaks at 834 and 727 cm^{-1}, which are related to the out-of-plane bending vibrations of C-H in aromatic rings with a large degree of substitution.[1]

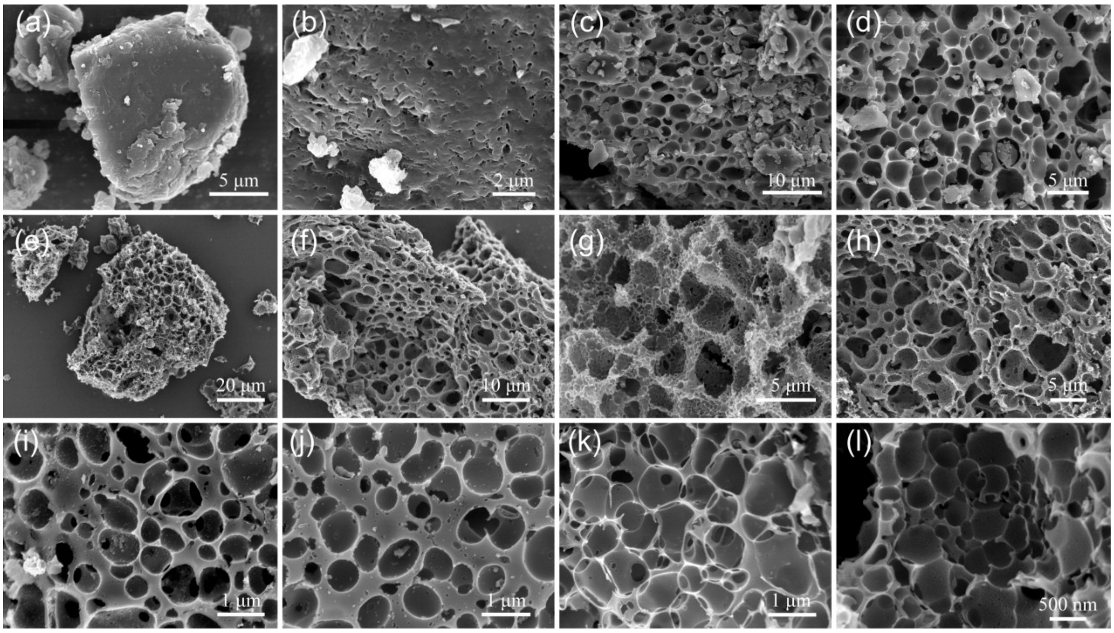

Fig. S2 (a) and (b) SEM image of the lignin precursor; (c) and (d) SEM image of the hydrochar pretreated at 180 °C; (e)-(l) SEM image of the LHCs.

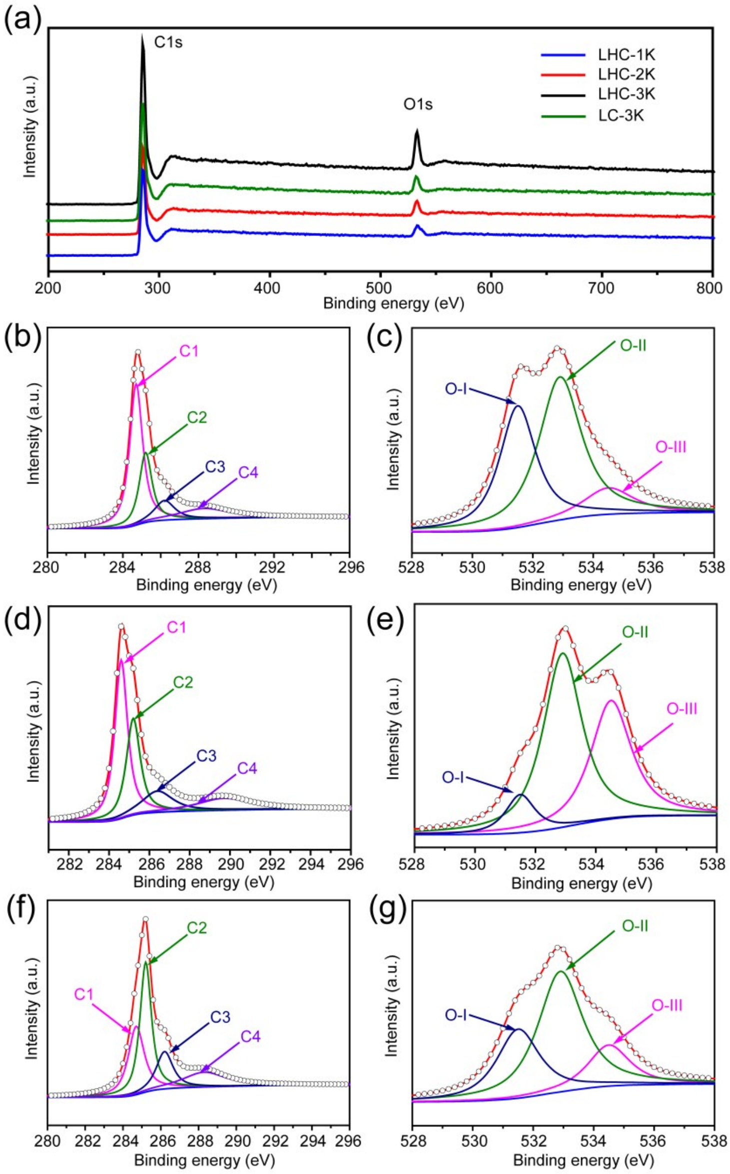

Fig. S3 (a) XPS spectra of LHCs and LC-3K; (b) C1s and (c) O1s of LHC-1K; (d) C1s and (e) O1s of LHC-2K; (f) C1s and (g) O1s of LC-3K.

Table S1. Yield, conductivity, textual parameters and surface element content of hydrochar, LC-3K and LHCs.

Sample	Yield	$^{a}S_{BET}$	$^{b}V_{total}$	$^{c}V_{micro}$	$^{d}V_{meso}$	Conductivity
	(%)	(m^2/g)	(cm^3/g)	(cm^3/g)	(cm^3/g)	S cm^{-1}
Hydrochar	55	8.9	0.02	0	0.01	--
LHC-1K	21	1290	0.59	0.55	0.02	5.4
LHC-2K	18	1355	0.62	0.56	0.04	5.2
LHC-3K	12	1660	0.78	0.66	0.10	4
LC-3K	3.8	1490	0.57	0.53	0.04	4.6

a: The specific surface area calculated by BET. b: total pore volume obtained by DFT. c: micropore volume calculated by DFT. d: mesopore volume calculated by DFT.

Table S2. The elemental composition of the lignin precursor, hydrochar, LC-3K and LHCs.

Sample	C	H	O	N	C	O
	wt.%	wt.%	wt.%	wt.%	at.%	at.%
Precursor	62.3	5.8	28.6	1.4	--	--
Hydrochar	69.4	6.1	22.8	1.0	--	--
LHC-1K	94.1	1.2	3.3	0.6	93.2	6.8
LHC-2K	92.9	1.5	4.4	0.7	92.8	7.1
LHC-3K	92.1	1.6	4.7	0.7	90.1	8.6
LC-3K	87.2	0.8	6.9	0.5	93.4	5.9

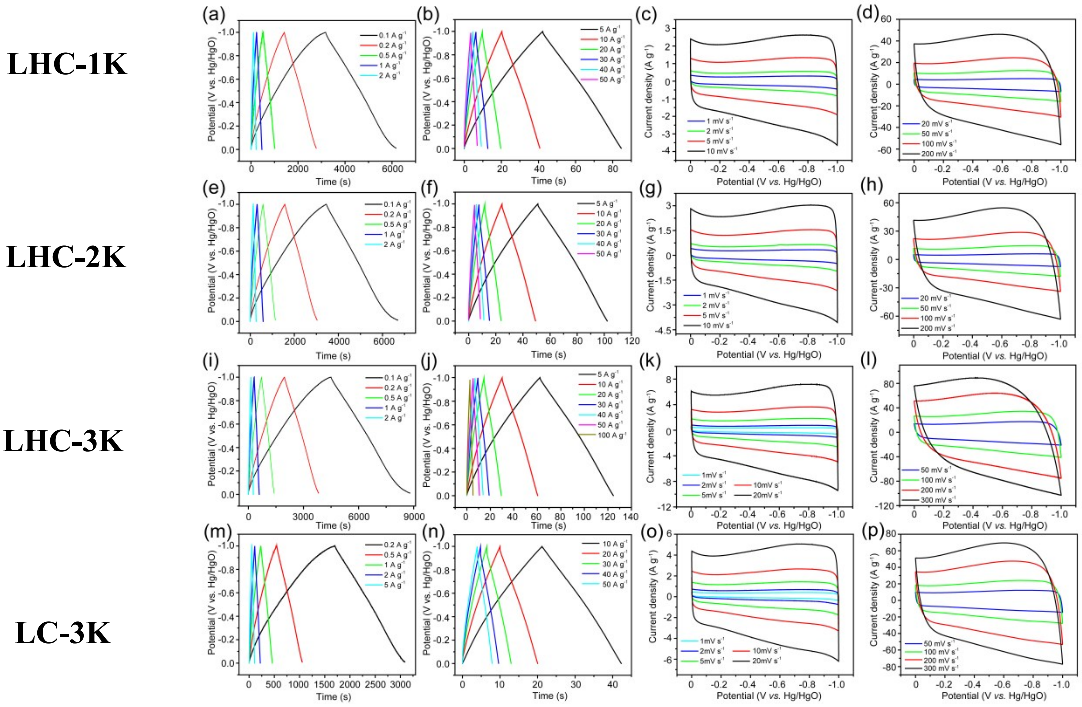

Fig. S4 (a), (b), (e), (f), (i), (j), (m) and (n) charge-discharge curves at different current densities; (c), (d), (g), (h), (k), (l), (o) and (p) cyclic voltammetry curves at different scan rates in a three-electrode system with 6 M KOH as electrolyte.

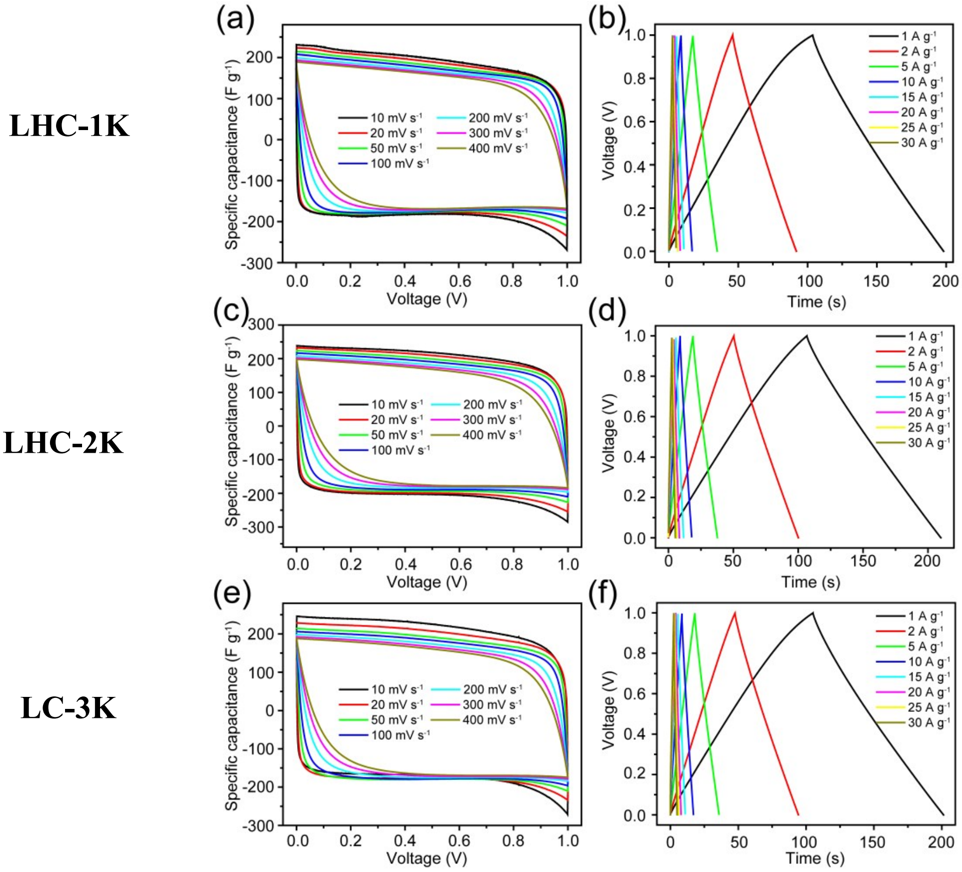

Fig. S5 (a), (c) and (e) Cyclic voltammetry curves at different scan rates; (b), (d) and (f) charge-discharge curves at different current densities in a two-electrode system with 6 M KOH aqueous solution.

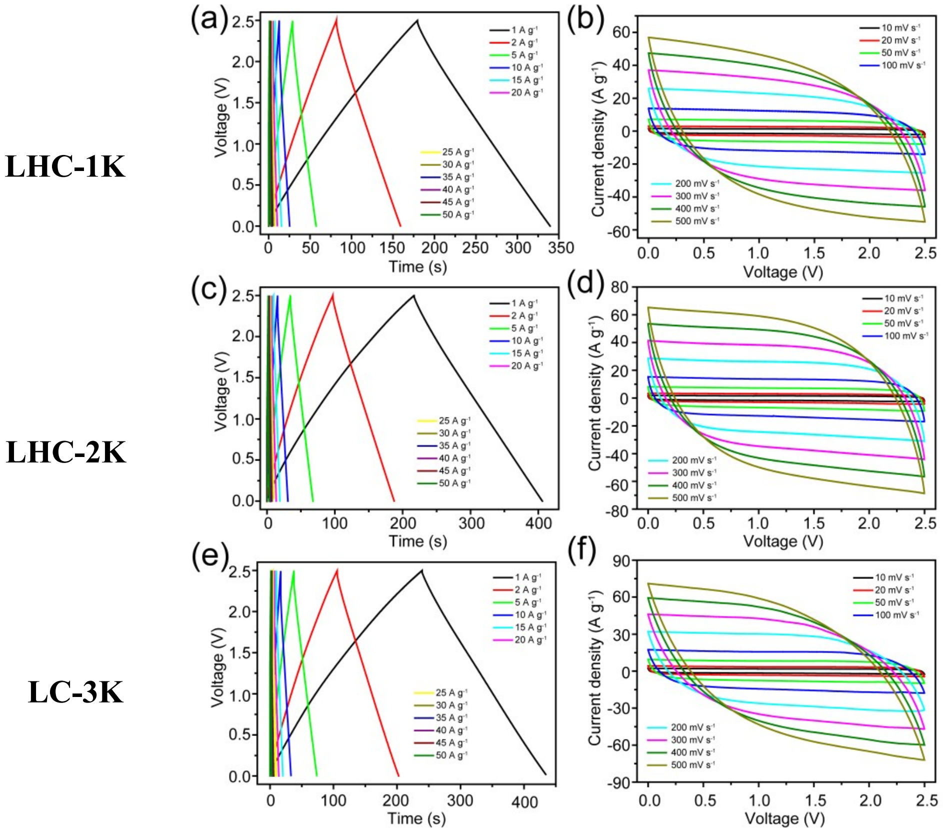

Fig. S6 (a), (c) and (e) Charge-discharge curves at different current densities; (b), (d) and (f) cyclic voltammetry curves at different scan rates in a two-electrode system with EMIM TFSI as electrolyte at 60 °C.

In this study, the gravimetric specific capacitance of a single electrode in two-electrode system was deduced from the charge-discharge curves according to the eqn (1):

$$C = \frac{2 * I * \triangle t}{m * \triangle V} \quad (1)$$

where I is the discharge current (A), $\triangle t$ is the discharge time (s), m is the mass of active material in the working electrode (g) and $\triangle V$ is the potential window (V). Energy density (E, Wh kg^{-1}) and power density (P, W kg^{-1}) based on the active electrode materials were calculated using eqn (2) and (3):

$$E = \frac{CV^2}{2 * 4 * 3.6} \quad (2)$$

$$P = \frac{3600 * E}{\triangle t} \quad (3)$$

where C (F g^{-1}) is the specific capacitance of single working electrode, V corresponds to the voltage change excluding the ohmic drop within Δt (V).

Table S3. Supercapacitances performance of various porous carbons reported in the representative literatures.

Materials	Two-electrode system			Ref.
	Capacitance ($F\ g^{-1}$)	Current density ($A\ g^{-1}$)	Electrolyte	
Hierarchical structured carbon	160	0.5	6 M KOH	Ref. 6
Nanoporous carbon	220 150	0.5 0.2	6 M KOH EMIM TFSI	Ref. 7
Carbon sheets	160	1	BMPY TFSI	Ref. 8
Activated carbon	195	0.5	6 M KOH	Ref. 9
Carbon nanosheets	208 135	0.5 0.1	1 M KOH 1 M Na_2SO_4	Ref. 10
Superactivated carbon	246 168	0.2 0.2	1 M H_2SO_4 EMIM FSI/AN	Ref. 11
Carbon flakes	143	0.1	1 M $LiPF_6$	Ref. 12
Biochar nanosheets	210	0.5	0.5 M H_2SO_4	Ref. 13
N-decorated porous carbon	205	0.5	6 M KOH	Ref. 14
Hierarchically porous carbons	238 149	0.2 0.2	6 M KOH 1 M TEA BF_4	Ref. 15
Porous Carbon Nanofibers	80	0.5	0.5 M H_2SO_4	Ref. 16
3D graphene	210	2	EMIM BF_4	Ref. 17
Activated graphene	164	1	BMIM BF_4/AN	Ref. 18
Activated carbon	136	1	EMIM BF_4/AN	Ref. 19
LHC-3K	**232** **218**	**0.5** **5**	**6 M KOH** **EMIM BF_4**	**This work**

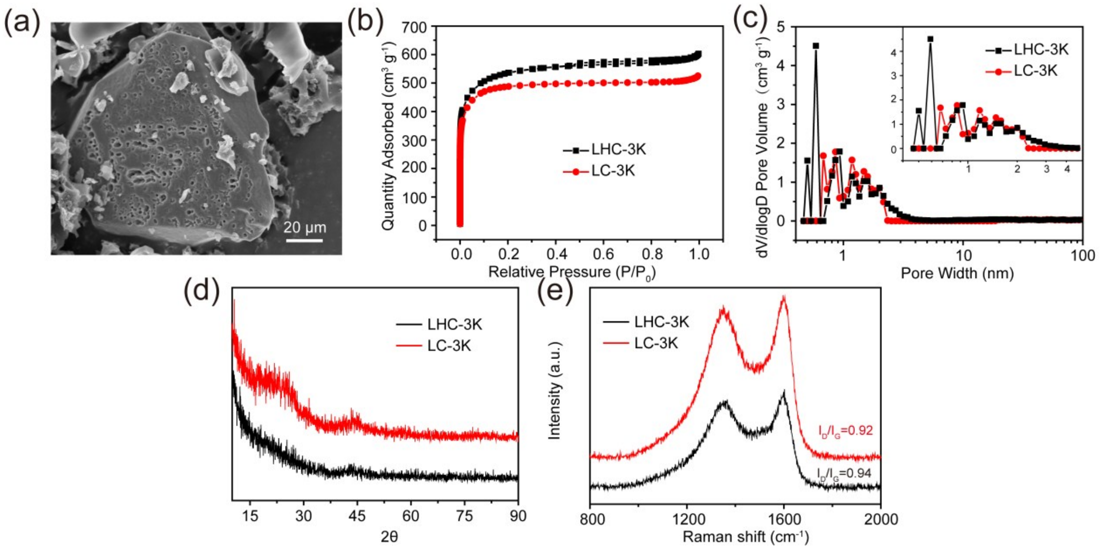

Fig. S7 (a) SEM image of LC-3K; (b) Nitrogen sorption isotherms and (c) the pore size distributions deduced by the DFT method; (d) XRD pattern and (e) Raman shift spectra of LC-3K and LHC-3K.

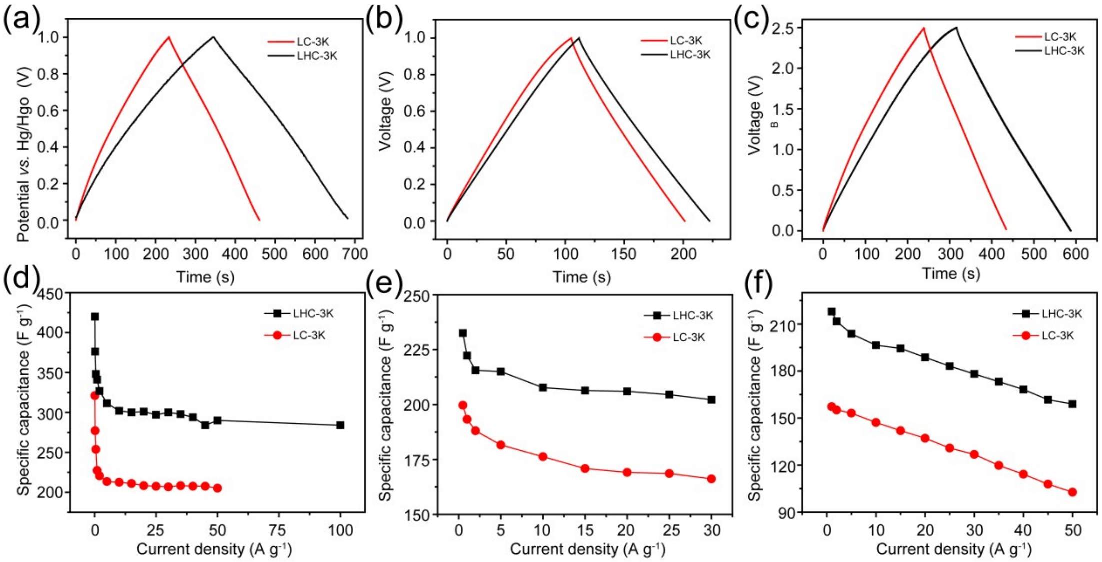

Fig. S8 (a), (b) and (c) Charge-discharge curves at 1A g^{-1}; (d), (e) and (f) rate performance of the LHC-3K and LC-3K based electrodes in three-electrode system, two-electrode system in 6 M KOH and two-electrode system in neat EMIM TFSI.

We also confirm the key role of the hydrothermal process to obtain hierarchical porous carbon. A control sample was prepared by directly activated lignin with KOH ($m_{KOH}/m_{lignin}=3$) in a horizontal tube furnace at 800 °C for 3h under nitrogen atmosphere at a heating rate of 5 °C min^{-1}. As seen in Fig. S7a, the SEM image of the control sample exhibit blocks structure and irregular holes structure different from the honeycomb and interconnected pores structure of LHC-3K, which demonstrates the hydrothermal carbonization process is a necessary step to convert lignin into 3D hierarchical porous carbons. The porous texture of control sample was measured by nitrogen adsorption/desorption experiments. The N_2 adsorption/desorption isotherm and the pore size distribution calculated by the DFT method are shown in Fig. S7b and c. The control sample owns a low quantity absorbed, suggesting specific surface area (1490 m^2 g^{-1}) is lower than that of LHC (1660 m^2 g^{-1}) and the control sample also show a very lower product yield (3.8%) than the total yield LHC-3K (55%*12%=6.6%). The pristine enzymatic hydrolysis lignin containing more volatiles was more severely affected by KOH activation. The volatile evolution would favour both the reaction of KOH with carbon at lower temperatures and the excess activation leading to a lower yield and surface area. [20, 21]

The XRD and Raman spectra show the amorphous structure of the control sample. Electrochemical characterization of the control sample is exhibited in Fig. S8. the control sample displays lower capacitance response and rate performance compared with that of the LHC-3K both in three-electrode system and two-electrode system in aqueous and ionic liquid electrolytes, which are attributed to the fact that the LHC-3K possesses a high specific surface area with 3D hierarchical porous structure to buffer vast electrolyte ions and thus owns an efficiently ion transfer process at high scan rates. In addition, LHC-3K possesses higher pore volume between 2 and 3 nm which the broader pore can allow plentiful electrolyte ions to easily extrude through the pores.[17] The porous structure leads to an obvious enhancement of specific capacitance because the plentiful electrolyte ions are extruded through the micropores and build an ion monolayer inside the micropore under a given potential. [7, 22]

Reference

1 R. Yang, G. Liu, X. Xu, M. Li, J. Zhang, X. Hao, Biomass and Bioenergy, 2011, 35, 437-445.

2 J. Guo, and A. C. Lua, Mater. Lett., 2002, 55, 334-339.

3 Z. M. Wang, H. Kanoh, K. Kaneko, G. Q. Lu and D. Do. Carbon, 2002, 40, 1231-1239.

4 Z. H. Hu, M. P. Srinivasan, and Y. M. Ni, Carbon, 2001, 39, 877-886.

5 F. Shafizadeh, J Anal. Appl. Pyrolysis, 1982, 4, 283-305.

6 H. Feng, H. Hu, H. Dong, Y. Xiao, Y. Cai,; B. Lei, Y. Liu, M. Zheng, J. Power Sources, 2016, 302, 164-173.

7 W. Tian, Q. Gao, Y. Tan, K. Yang, L. Zhu, C. Yang, and H. Zhang, J. Mater. Chem. A, 2015, 3, 5656-5664.

8 H. Wang, Z. Xu, A. Kohandehghan, Z. Li, K. Cui, X. Tan, T. J. Stephenson, C. K. King'ondu, C. M. B. Holt, B. C. Olsen, J. K. Tak, D. Harfield, A. O. Anyia, D. Mitlin, ACS Nano, 2013, 7, 5131-5141.

9 F. Gao, J. Qu, Z. Zhao, Z. Wang, J. Qiu, Electrochimica Acta, 2016, 190, 1134-1141.

10 H. Peng, G. Ma, K. Sun, Z. Zhang, Q. Yang, Z. Lei, Electrochimica Acta, 2016, 90,

862-871.

11 M. Sevilla, G. A. Ferrero, A. B. Fuertes, Carbon, 2017, 114, 50-58.

12 W. Qian, F. Sun, Y. Xu, L. Qiu, C. Liu, S. Wang, F. Yan, Energy Environ. Sci. 2014, 7, 379-386.

13 M. Genovese, J. Jiang, K. Lian, N. Holmb, J. Mater. Chem. A, 2015, 3, 2903-2913.

14 F. Gao, J. Qu, C. Geng, G. Shao, M. Wu, J. Mater. Chem. A, 2016, 4, 7445-7452.

15 P. Cheng, S. Gao, P. Zang, X. Yang, Y. Bai, H. Xu, Z. Liu, Z. Lei, Carbon, 2015, 93, 315-324.

16 Y. Liu, J. Zhou, L. Chen, P. Zhang, W. Fu, H. Zhao, Y. Ma, X. Pan, Z. Zhang, W. Han, E. Xie, ACS Appl. Mater. Interfaces, 2015, 7, 23515-23520.

17 L. Zhang, F. Zhang, X. Yang, G. Long, Y. Wu, T. Zhang, K. Leng, Y. Huang, Y. Ma, A. Yu, Scientific Reports, 2013, 3, 1408.

18 M. Sevilla and A.B. Fuertes. Chem. Sus. Chem., 2016, 9,1880-1888.

19 Y. Zhu, S. Murali, M. D. Stoller, K. J. Ganesh, W. Cai, P. J Ferreira, A. Pirkle, R. M. Wallace, K. A. Cychosz, M. Thommes, D. Su, E. A. Stach, R. S. Ruoff, Science, 2011;332, 1537-1541.

20 S. Schaefer, V. Fierro, M. T. Izquierdo, A. Celzard, 2016, 41, 12146-12156.

21 M. A. Lillo-Ródenas, J. P. Marco-Lozar, D.Cazorla-Amoros, A. Linares-Solano, 2007, 80, 166-174.

22 L. Wei, M. Sevilla, A. B. Fuertes, R. Mokaya and G. Yushin, Adv. Energy Mater., 2011, 1, 356-361.